

Low-Profile Dual-Band Shared-Aperture Base Station Antennas Based on FSS Radiators

Hui Li , Senior Member, IEEE, Jiawen Xu , Yang Nan , Qiang Chen , and Changfei Zhou 

Abstract—In this letter, a low-profile dual-band dual-polarized base station antenna system is proposed for 5G applications. Distinct from previous base station antennas using FSS as a decoupling layer, the frequency selective surface (FSS) structure is employed directly as the low-band (LB) antenna at 0.69–0.96 GHz. At the same time, the FSS operates as the reflector for the high-band (HB) antennas at 3.3–3.8 GHz. Hence, the radiation patterns of both the HB and the LB antennas are restored to match the patterns of the isolated antennas. Stable radiation and high boresight gains are achieved over the operating bands. The antennas are fabricated and measured, with the measurement results agreeing well with the simulated ones. The proposed antenna array is suitable for base stations with large-scale arrays due to its simple structure, low profile and stable radiation features.

Index Terms—Base station antennas, dual-polarized antennas, frequency selective surface (FSS), multiple-input–multiple-output (MIMO) antennas, shared-aperture antennas.

I. INTRODUCTION

THE fifth-generation communication system has demonstrated the capacity to deliver extensive connectivity, high throughput, and low latency [1], [2], [3], [4], [5], [6]. It becomes imperative to equip base stations with simultaneous support for 2G, 3G, and 4G/5G bands. Though a single antenna can cover dual or even multiple frequency bands [7], [8], [9], it is difficult to achieve stable radiation characteristics over all the bands. To provide constant radiation features, antennas of different dimensions are normally stacked together to operate at their fundamental resonances [10], [11], [12], [13], [14], [15], [16], yet resulting in high mutual coupling and high profile. Two popular arrangements for shared-aperture antenna arrays are depicted in Fig. 1(a) and (b), respectively. In Fig. 1(a), the high-band (HB) antennas are located below the LB antennas, whereas the low-band (LB) antenna is placed at the lower layer in Fig. 1(b). In both schemes, high isolations are in demand between the antennas at different bands.

Recently, decoupling methods have been extensively studied for shared-aperture antennas [17], [18], [19], [20], [21], [22], [23], [24], [25], [26], [27], [28], [29], [30]. Once the low band

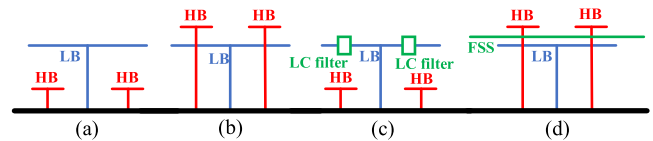


Fig. 1. Shared-aperture antenna structures: (a) LB–HB scheme; (b) HB–LB scheme; (c) LB–HB scheme with LC filter; (d) HB–LB scheme with FSS.

antenna is placed at the upper layer [18], [19], [20], [21], [22], [23], [24], [25], [26], it is challenging to design the LB antenna as an electromagnetic transparent antenna at the HB. Various kinds of choke structures have been proposed to suppress the mutual coupling between the LB and the HB antennas, as shown in Fig. 1(c). In [18], a cascaded comb dipole antenna has been utilized in the LB to counteract the currents induced by the HB antenna, thereby suppressing the secondary radiation.

For the configuration with the HB antennas at the upper layer, as shown in Fig. 1(b), the primary focus is on maintaining consistent reflection properties of the LB antenna for the HB antennas. The introduction of frequency selective surface (FSS) structures is a common practice to achieve the reflection [27], [28], [29], [30] and reduce the profile, as illustrated in Fig. 1(d). In [30], FSS has been initially employed to decouple the HB and LB antennas, effectively mitigating their interference. However, it is important to note that the placement of the FSS between the HB and LB antennas introduces certain complexities into the system and poses stability challenges.

In this letter, the LB antenna is designed as an FSS surface to provide low transmission characteristics in the HB, so that the LB antenna acts as a ground plane for the HB antenna. This way, dual-layer dual-band shared-aperture antennas with restored radiation patterns are retained. The antenna array consists of an LB antenna at 0.69–0.96 GHz and four HB antennas at 3.3–3.8 GHz. Boresight radiations with the realized gains of 9 dBi and 8.3 dBi have been achieved, respectively, for the LB and the HB antennas. The lateral size of the antenna has been reduced by $0.2\lambda_g$ compared with conventional FSS-based structures.

II. DUAL-BAND SHARED-APERTURE ANTENNAS

A. Antenna Configurations

Conventionally, the FSS structure is employed between the LB antenna and the HB antennas, achieving high-frequency stopband and low-frequency passband at the base station [27], [30]. In this scheme, a part of the power radiated by the LB antenna is reflected by the FSS, resulting in a slightly lower efficiency of the LB antenna. Moreover, the antenna system becomes complicated with an extra FSS layer. In contrast, in

Manuscript received 26 January 2024; accepted 28 February 2024. Date of publication 5 March 2024; date of current version 4 June 2024. This work was supported in part by the National Natural Science Foundation of China under Grant 62371089, in part by Dalian Excellent Young Science and Technology Talents Project 2023RY015, and in part by Fundamental Research Funds for the Central Universities DUT23YG111. (Corresponding author: Hui Li.)

Hui Li, Jiawen Xu, Yang Nan, and Changfei Zhou are with the School of Information and Communication Engineering, Dalian University of Technology, Dalian 116024, China (e-mail: hui.li@dut.edu.cn).

Qiang Chen is with the Research Institute of Electrical Communication, Tohoku University, Sendai 980-8577, Japan.

Digital Object Identifier 10.1109/LAWP.2024.3372529

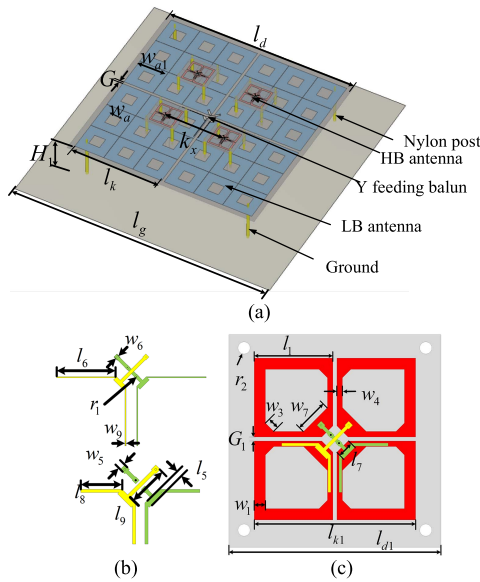


Fig. 2. (a) Configurations of the proposed dual-band dual-polarized shared-aperture antenna system. (b) Y-shaped feedings. (c) HB antenna. ($l_d = 211.2$, $w_{a1} = 34$, $w_a = 13$, $G = 3$, $l_k = 91$, $l_6 = 27$, $l_8 = 6$, $w_6 = 2$, $l_5 = 2.78$, $l_9 = 5.5$, $w_9 = 0.5$, $r_1 = 0.15$, $r_2 = 2$, $l_1 = 13$, $w_7 = 5.6$, $w_4 = 0.92$, $l_7 = 2.78$, $w_1 = 1.86$, $l_{k1} = 26.65$, $l_{d1} = 35$, $l_g = 500$, $G_1 = 2$, $w_3 = 2$, $k_x = 68$, $k_y = 68$, $H_1 = 45$, $H_2 = 17$, unit: mm.)

this work, the FSS structure operates as the main radiator at the LB. Therefore, the number of layers is reduced, leading to simpler structures.

Fig. 2(a) shows the overall configurations of the proposed dual-band shared-aperture antenna system, which is composed of one LB antenna and four HB antennas, with the HB antennas placed above the LB antenna. The LB antenna is composed of two orthogonal dipole antennas with $\pm 45^\circ$ polarizations, which are built from FSS units. The low-band antenna, as shown in Fig. 2(a), consists of orthogonal dipoles with square-loop radiating arms, which is similar to conventional base station antennas in [31]. Each radiating arm of the dipole is constructed by 3×3 units, leading to a 6×6 FSS structure. The LB FSS-based antenna is capacitively fed by the Y-shaped strips printed on the other side of the substrate, with the details given in Fig. 2(b). In each central FSS unit of the dipole arm, a square hole is etched in the center. The LB FSS-based antenna is printed on the dielectric substrate of FR-4, with a dielectric constant of 4.4, a loss tangent of 0.02, and a thickness of 0.8 mm. In the HB, the FSS structures work as a reflector. In order to simulate the real situation in the base station, a large ground plane with the dimensions of $500 \text{ mm} \times 500 \text{ mm}$ is utilized.

Fig. 2(c) shows the configurations of the HB antenna, consisting of two orthogonal loop dipoles with $\pm 45^\circ$ polarizations [31]. The dielectric substrate for the HB antenna is F4B, with a dielectric constant of 2.2, a loss angle tangent of 0.005 and a thickness of 0.8 mm. The height of the LB and HB antennas are 45 mm and 17 mm, respectively, and they are fixed with nylon posts at the corners.

B. Bandstop FSS at HB

To enable the FSS structure to work as a reflector at the HB, the FSS unit is first investigated. A rectangular patch unit is designed and placed on the dielectric substrate of FR-4, as shown in Fig. 3(a). A plane wave with 45° polarization is utilized to

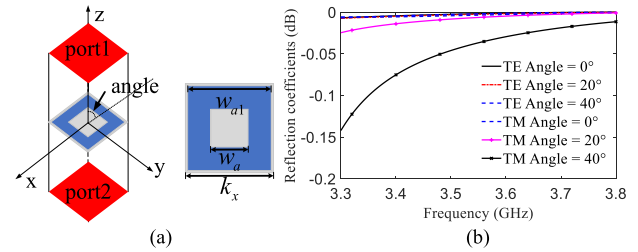


Fig. 3. (a) Setup for calculating the reflection coefficients of the FSS unit. (b) Reflection coefficients of the FSS in the high band.

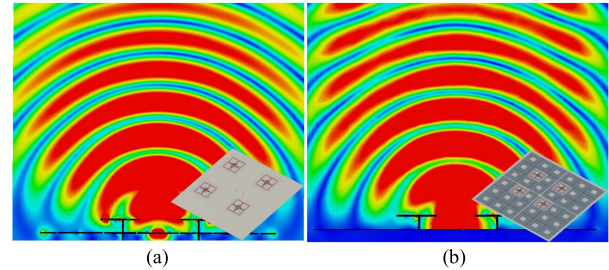


Fig. 4. Electric field distributions of the HB antenna at 3.5 GHz on (a) ground plane made of PEC and (b) FSS.

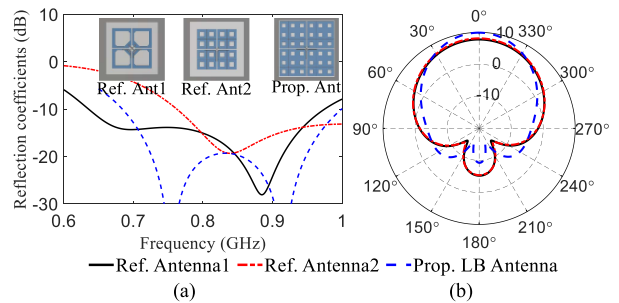


Fig. 5. Evolution of the proposed antennas: (a) reflection coefficients; (b) radiation patterns.

excite the FSS unit, with the periodic boundary applied. The reflection coefficients of the FSS unit in the HB are displayed in Fig. 3(b). In the HB, the reflection coefficients are above -0.2 dB , which reveals excellent reflection characteristics of the FSS.

In order to validate the reflection characteristics of the proposed FSS below the real HB antennas, the E -field distributions on the $\varphi = 45^\circ$ plane for the HB antennas on the PEC and on the FSS structures are compared in Fig. 4. Compared with the HB antenna on PEC, the E -fields are only slightly distorted, which indicates that the proposed FSS has almost the same reflection ability as the ideal ground plane for the HB antennas. Still, a slightly larger back lobe is observed for the HB antenna due to nonperfect reflection. The gain remains almost unchanged.

C. Designs of the LB Antenna

The design process of the LB antenna is shown in Fig. 5(a), which has evolved from a typical loop-dipole antenna, as given by reference antenna 1 in Fig. 5(a). As illustrated in [32], the two resonances are attributed to the strong mutual coupling between the radiating dipole and the parasitic dipole. Though the

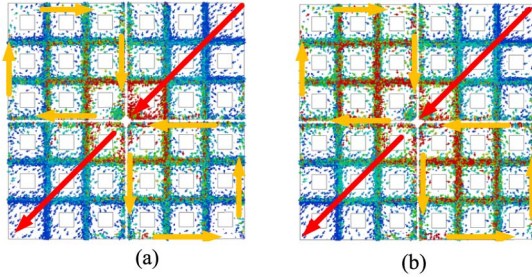


Fig. 6. Surface currents for the dual-polarized dipole at (a) 0.7 and (b) 1 GHz.

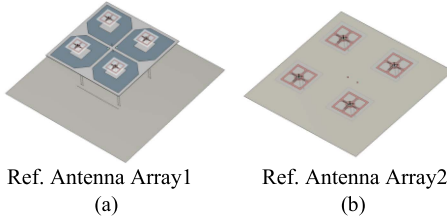


Fig. 7. Reference antenna arrays: (a) original LB-HB antennas without FSS; (b) HB antennas on ideal ground plane.

two orthogonal dipoles are coupled to each other, the isolations are very high since currents on the parasitic dipole are strictly symmetrical with respect to its center, leading to no voltage difference at its feeding.

To form the FSS structure with band-stop characteristics, each square loop is split into 2×2 square rings, with each unit the same as the one in Fig. 3(a). The chamfers are removed to keep all the FSS units identical. The lateral dimensions of the HB antennas are maintained unchanged. The reflection coefficients of the reference antennas are presented in Fig. 5(a). Compared with reference antenna 1, reference antenna 2 resonates at a higher frequency due to the shorter electric length of the antenna when the loops are filled by more conducting material. Fortunately, the radiation patterns of the two reference antennas are almost identical, as presented in Fig. 5(b) on the $\varphi = 45^\circ$ plane.

To move down the resonance of the LB antenna to the target band, each loop of the LB radiator is expanded to a 3×3 FSS structure, without changing the size of the FSS unit. Consequently, the resonance is moved back to 0.69–0.96 GHz, as given in Fig. 5(a). The capacitive coupling between the FSS units replaces the capacitive loading of the FSS in [30]. Therefore, the proposed antenna provides good impedance matching, though the profile is low. Compared with the reference antennas, the proposed LB antenna provides a higher gain but a narrower 3 dB beamwidth due to the larger antenna aperture. The current distributions of the LB FSS-based radiators at 0.7 and 1 GHz are given in Fig. 6.

To investigate the performance of the proposed HB antennas, two other antenna array setups are investigated. The first setup includes the conventional LB and HB antennas on the ground plane without any FSS structure or chokes [33], as given in Fig. 7(a). In the second setup, the HB antennas are simply placed above the ground plane, as shown in Fig. 7(b).

Fig. 8 displays the radiation patterns of the HB antennas at different frequencies over the operating band in different setups. Compared with the HB antennas on the ground plane, the radiation pattern of the HB antenna in the first setup is severely distorted by the LB antenna, resulting in a smaller beamwidth and a lower gain. With the proposed LB radiator built from FSS

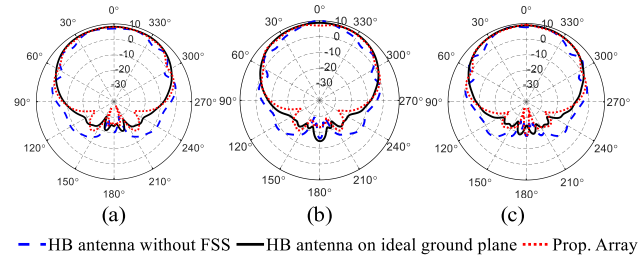


Fig. 8. Radiation patterns of the HB antennas for the reference antenna and the proposed antenna at (a) 3.3, (b) 3.5, and (c) 3.8 GHz.

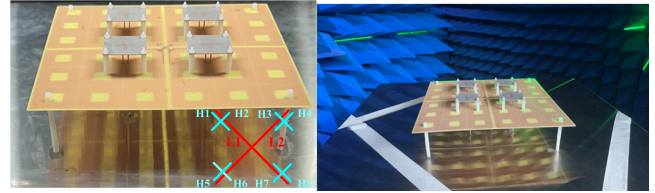


Fig. 9. (a) Antenna prototype. (b) Measurement setup of the proposed base station antenna system.

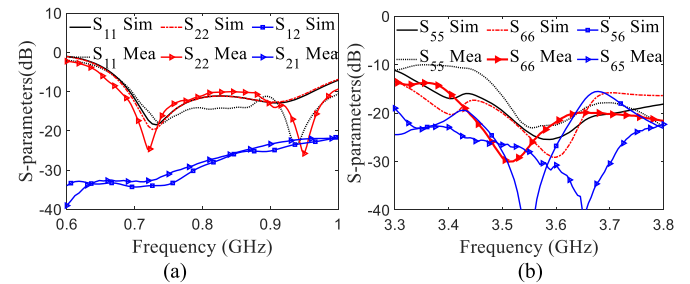


Fig. 10. Simulated and measured S -parameters for the proposed base station antenna system: (a) LB antenna; (b) HB antenna.

structures, the radiation pattern of the HB antennas has been effectively restored, which is almost identical to that on the ideal ground plane.

The HB antennas above have limited impact on the radiation of the LB antennas, as they are electrically small. When more HB antennas are implemented, pattern distortion would appear due to the mutual coupling between HB antennas.

III. MEASUREMENT RESULTS AND DISCUSSIONS

To validate the proposed method, a prototype of the base station antenna array was fabricated and measured, as shown in Fig. 9(a). Air holes were drilled on the substrate of both the LB and the HB antennas, and nylon was used to support the antennas. The simulated and measured S -parameters of the proposed antenna array were presented in Fig. 10, showing good agreements for both the LB and the HB antennas. The measured and simulated bandwidths of the LB antenna with different polarizations covered 0.69–0.96 GHz, as shown in Fig. 10(a). For the HB antennas, ports 5 and 6 were selected as the representatives for the demonstration, whose bandwidth covered 3.3–3.8 GHz. The simulated and measured isolations of the LB antennas were above 20 dB, whereas the isolations were above 15 dB for the HB antennas.

The radiation patterns of the antennas were measured in the anechoic chamber, with the measurement setup given in

TABLE I
 COMPARISONS WITH OTHER SHARED-APERTURE BASE STATION ANTENNAS

Ref.	Design method	Array size ($\lambda_L \times \lambda_L \times \lambda_L$)*	Double-/Multi-layers	Mea-HPBW (variation)	Bandwidth	Gain (dBi)
[27]	FSS	0.69×0.69×0.14	Multi	5°/25°	0.69–0.96 GHz/3.3–3.8 GHz	8.3/6.5 dBi
[29]	FSS	1.13×1.13×0.41	Multi	Not Given	1.7–2.4 GHz/3.3–3.8 GHz	8/7.2 dBi
[30]	FSS	0.68×0.68×0.14	Multi	14°/40°	0.69–0.96 GHz/3.3–4.9 GHz	8.8/8.3 dBi
[33]	Filter	0.41×0.41×0.2	Double	10°/11°	0.69–0.96 GHz/3.3–3.8 GHz	8.7/8.1 dBi
[20]	Filter	0.41×0.41×0.184	Double	5°/16°	0.69–0.96 GHz/3.3–3.8 GHz	7/10.2 dBi
[17]	Filter	0.5×0.5×0.23	Double	10°/16°	1.9–2.5 GHz/3.3–3.9 GHz	9.1/7.5 dBi
Prop. Ant.	FSS	0.48×0.48×0.14	Double	8°/14°	0.69–0.96 GHz/3.3–3.8 GHz	9/8.3 dBi

* λ_L is the free-space wavelength at the lowest frequency in LB.

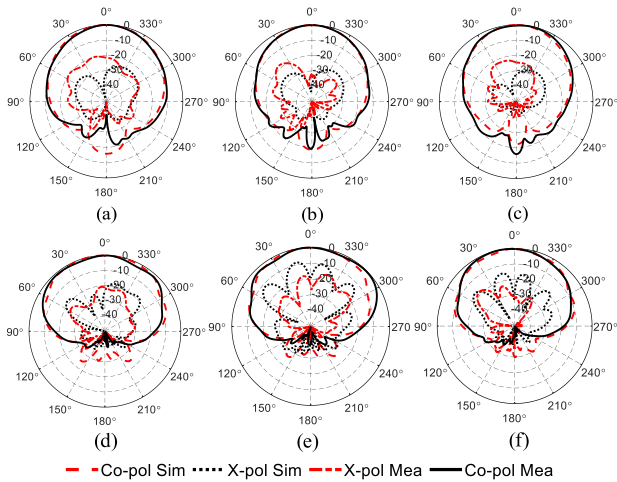


Fig. 11. Measured and simulated radiation patterns of the antenna array. (a) 0.69 GHz. (b) 0.85 GHz. (c) 0.96 GHz. (d) 3.3 GHz. (e) 3.5 GHz. (f) 3.8 GHz.

Fig. 9(b). Fig. 11 shows the radiation patterns of the LB and HB antennas, with representative frequencies selected at 0.69, 0.85, and 0.96 GHz in the LB and 3.3, 3.5, and 3.8 GHz in the HB. Due to the symmetry of the antenna array, only radiation patterns with $\pm 45^\circ$ polarizations (port L1 and port H4) were presented to facilitate a clear comparison between the simulated and measured results. In general, there was a strong agreement between the measured and simulated radiation patterns. As depicted in Fig. 11(a)–(c), the LB antenna maintained a stable radiation pattern across the operating band, with the measured XPD consistently exceeding 20 dB. Furthermore, with the FSS structure serving as the reflector, the HB antenna exhibited a stable unidirectional boresight radiation pattern as well. In the HB, the measured cross-polarization levels were a bit higher than the simulated ones due to the cable influence.

Fig. 12 shows the simulated and measured gains as well as the beamwidth of the LB and HB antennas over the operating band. In the LB, the averaged measured gain was around 0.5 dB lower than the simulated ones, and the measured gain varied within the range of 9 ± 0.3 dBi, which was relatively high and stable. The HPBW ranged from 60° to 68° . In the HB, the measured gains fell in the range of 8.3 ± 0.7 dBi, with the HPBW between 86° and 100° . The stable performances of both antennas make the proposed system suitable for base station applications.

The proposed antennas are compared with the state-of-the-art dual-polarized co-aperture antenna arrays in the literature in Table I. All the antenna systems under comparison consist of one LB antenna and four HB antennas. In [27], [29], and [30],

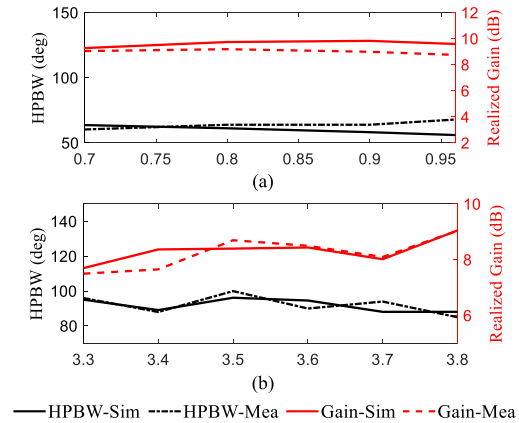


Fig. 12. Measured and simulated realized gains and HPBWs in (a) the LB and (b) in the HB.

FSS structures have been utilized between the LB and HB antennas to enhance radiation performance. Despite the increased number of antenna layers, the overall profile has been reduced compared with the antennas with filter structures [17], [20], [33]. Compared with the antennas with intermediate FSS structures, the lateral size of the proposed design and HPBW have been greatly reduced. At the same time, the variations of the HPBW at the high band are significantly improved due to the stable radiation patterns. Compared with the filter-based antennas, although the lateral size of our proposed antenna is slightly larger due to the FSS structure serving as the radiator, a nearly 50% reduction in profile has been achieved while maintaining similar HPBW and gains at both frequency bands. Consequently, the proposed antenna system outperforms the existing schemes in terms of low profile, simple structure and stable radiation patterns.

IV. CONCLUSION

In this letter, a distinct scheme has been proposed for designing co-aperture base station antennas. Unlike conventional cross-dipole antennas, the FSS structure has been employed as the radiator at the LB, and at the same time as the reflector for the HB antennas. With simply two layers, the HB and LB antennas have been well decoupled without pattern distortion. The gains of the LB antenna and the HB antennas vary within the ranges of 9 ± 0.3 dBi and 8.3 ± 0.7 dBi, respectively, exhibiting stable radiation features. The proposed scheme is suitable for base stations due to its simple structure and outstanding radiation features. In the future, more efforts will be made to reduce the profile of the HB antennas.

REFERENCES

- [1] A. Gupta and R. K. Jha, "A survey of 5G network: Architecture and emerging technologies," *IEEE Access*, vol. 3, pp. 1206–1232, 2015.
- [2] M. Shafi et al., "5G: A tutorial overview of standards, trials, challenges, deployment, and practice," *IEEE J Sel. Areas Commun.*, vol. 35, no. 6, pp. 1201–1221, Jun. 2017.
- [3] A. Alieldin, Y. Huang, S. J. Boyes, M. Stanley, S. D. Joseph, and B. Al-Juboori, "A dual-broadband dual-polarized Fyffot-shaped antenna for mobile base stations using MIMO over-lapped antenna subarrays," *IEEE Access*, vol. 6, pp. 50260–50271, 2018.
- [4] H. Q. Ngo, E. G. Larsson, and T. L. Marzetta, "Energy and spectral efficiency of very large multiuser MIMO systems," *IEEE Trans. Commun.*, vol. 61, no. 4, pp. 1436–1449, Apr. 2013.
- [5] H. Huang, X. Li, and Y. Liu, "A low-profile, dual-polarized patch antenna for 5G MIMO application," *IEEE Trans. Antennas Propag.*, vol. 67, no. 2, pp. 1275–1279, Feb. 2019.
- [6] H. Huang, X. Li, and Y. Liu, "5G MIMO antenna based on vector synthetic mechanism," *IEEE Antennas Wireless Propag. Lett.*, vol. 17, no. 6, pp. 1052–1055, Jun. 2018.
- [7] Y. Liu, S. Wang, N. Li, J.-B. Wang, and J. Zhao, "A compact dual-band dual-polarized antenna with filtering structures for sub-6 GHz base station applications," *IEEE Antennas Wireless Propag. Lett.*, vol. 17, no. 10, pp. 1764–1768, Oct. 2018.
- [8] Y. Li, Z. Zhao, Z. Tang, and Y. Yin, "Differentially fed, dual-band dual-polarized filtering antenna with high selectivity for 5G sub-6 GHz base station applications," *IEEE Trans. Antennas Propag.*, vol. 68, no. 4, pp. 3231–3236, Apr. 2020.
- [9] H. Huang, Y. Liu, and S. Gong, "A dual-broadband, dual-polarized base station antenna for 2G/3G/4G applications," *IEEE Antennas Wireless Propag. Lett.*, vol. 16, pp. 1111–1114, 2017.
- [10] Y. He, Y. Yue, L. Zhang, and Z. N. Chen, "A dual-broadband dual-polarized directional antenna for all-spectrum access base station applications," *IEEE Trans. Antennas Propag.*, vol. 69, no. 4, pp. 1874–1884, Apr. 2021.
- [11] F. Jia, S. Liao, and Q. Xue, "A dual-band dual-polarized antenna array arrangement and its application for base station antennas," *IEEE Antennas Wireless Propag. Lett.*, vol. 19, no. 6, pp. 972–976, Jun. 2020.
- [12] R. Wu and Q. X. Chu, "A compact, dual-polarized multiband array for 2G/3G/4G base stations," *IEEE Trans. Antennas Propag.*, vol. 67, no. 4, pp. 2298–2304, Apr. 2019.
- [13] X. Liu et al., "A mutual-coupling-suppressed dual-band dual-polarized base station antenna using multiple folded-dipole antenna," *IEEE Trans. Antennas Propag.*, vol. 70, no. 12, pp. 11582–11594, Dec. 2022.
- [14] L. Y. Nie et al., "A low-profile coplanar dual-polarized and dual-band base station antenna array," *IEEE Trans. Antennas Propag.*, vol. 66, no. 12, pp. 6921–6929, Dec. 2018.
- [15] Y. He, Z. Pan, X. Cheng, Y. He, J. Qiao, and M. M. Tentzeris, "A novel dual-band, dual-polarized, miniaturized and low-profile base station antenna," *IEEE Trans. Antennas Propag.*, vol. 63, no. 12, pp. 5399–5408, Dec. 2015.
- [16] Y. Chen, J. Zhao, and S. Yang, "A novel stacked antenna configuration and its applications in dual-band shared-aperture base station antenna array designs," *IEEE Trans. Antennas Propag.*, vol. 67, no. 12, pp. 7234–7241, Dec. 2019.
- [17] Y. Da, X. Chen, and A. A. Kishk, "In-band mutual coupling suppression in dual-band shared-aperture base station arrays using dielectric block loading," *IEEE Trans. Antennas Propag.*, vol. 70, no. 10, pp. 9270–9281, Oct. 2022.
- [18] X. Lu, Y. Chen, S. Guo, and S. Yang, "An electromagnetic-transparent cascade comb dipole antenna for multi-band shared-aperture base station antenna array," *IEEE Trans. Antennas Propag.*, vol. 70, no. 4, pp. 2750–2759, Apr. 2022.
- [19] W. Niu, B. Sun, G. Zhou, and Z. Lan, "Dual-band aperture shared antenna array with decreased radiation pattern distortion," *IEEE Trans. Antennas Propag.*, vol. 70, no. 7, pp. 6048–6053, Jul. 2022.
- [20] J. Jiang and Q.-X. Chu, "Dual-band shared-aperture base station antenna array based on 3-D chokes," *IEEE Antennas Wireless Propag. Lett.*, vol. 22, no. 4, pp. 824–828, Apr. 2023.
- [21] S. J. Yang, Y. Yang, and X. Y. Zhang, "Low scattering element-based aperture-shared array for multiband base stations," *IEEE Trans. Antennas Propag.*, vol. 69, no. 12, pp. 8315–8324, Dec. 2021.
- [22] S. J. Yang, R. Ma, and X. Y. Zhang, "Self-decoupled dual-band dual-polarized aperture-shared antenna array," *IEEE Trans. Antennas Propag.*, vol. 70, no. 6, pp. 4890–4895, Jun. 2022.
- [23] G. N. Zhou, B. H. Sun, Q.-Y. Liang, S. T. Wu, Y. H. Yang, and Y. M. Cai, "Triband dual-polarized shared-aperture antenna for 2G/3G/4G/5G base station applications," *IEEE Trans. Antennas Propag.*, vol. 69, no. 1, pp. 97–108, Jan. 2021.
- [24] Y. L. Chang and Q. X. Chu, "Suppression of cross-band coupling interference in tri-band shared-aperture base station antenna," *IEEE Trans. Antennas Propag.*, vol. 70, no. 6, pp. 4200–4214, Jun. 2022.
- [25] Y. Li and Q. X. Chu, "Self-decoupled dual-band shared-aperture base station antenna array," *IEEE Trans. Antennas Propag.*, vol. 70, no. 7, pp. 6024–6029, Jul. 2022.
- [26] R. C. Dai, H. Su, S. J. Yang, J. H. Ou, and X. Y. Zhang, "Broadband electromagnetic-transparent antenna and its application to aperture-shared dual-band base station array," *IEEE Trans. Antennas Propag.*, vol. 71, no. 1, pp. 180–189, Jan. 2023.
- [27] D. He, Y. Chen, and S. Yang, "A low-profile triple-band shared-aperture antenna array for 5G base station applications," *IEEE Trans. Antennas Propag.*, vol. 70, no. 4, pp. 2732–2739, Apr. 2022.
- [28] Y. Zhu, Y. Chen, and S. Yang, "Integration of 5G rectangular MIMO antenna array and GSM antenna for dual-band base station applications," *IEEE Access*, vol. 8, pp. 63175–63187, 2020.
- [29] Y. Zhu, Y. Chen, and S. Yang, "Cross-band mutual coupling reduction in dual-band base-station antennas with a novel grid frequency selective surface," *IEEE Trans. Antennas Propag.*, vol. 69, no. 12, pp. 8991–8996, Dec. 2021.
- [30] Y. Zhu, Y. Chen, and S. Yang, "Decoupling and low-profile design of dual-band dual-polarized base station antennas using frequency-selective surface," *IEEE Trans. Antennas Propag.*, vol. 67, no. 8, pp. 5272–5281, Aug. 2019.
- [31] Q. X. Chu, D. L. Wen, and Y. Luo, "A broadband $\pm 45^\circ$ dual-polarized antenna with Y-shaped feeding lines," *IEEE Trans. Antennas Propag.*, vol. 63, no. 2, pp. 483–490, Feb. 2015.
- [32] Z. Bao, Z. Nie, and X. Zong, "A novel broadband dual-polarization antenna utilizing strong mutual coupling," *IEEE Trans. Antennas Propag.*, vol. 62, no. 1, pp. 450–454, Jan. 2014.
- [33] Y. Li and Q. X. Chu, "Coplanar dual-band base station antenna array using concept of cavity-backed antennas," *IEEE Trans. Antennas Propag.*, vol. 69, no. 11, pp. 7343–7354, Nov. 2021.